Physical ageing of amorphous and semicrystalline poly(ethylene terephthalate)

G. Vigier* and J. Tatibouet
INSA Bat.502, UA CNRS 341, GEMPPM, F69621 Villeurbanne Cedex, France
(Received 18 January 1993)

Thermal and micromechanical properties of amorphous and semicrystalline poly(ethylene terephthalate) are found to be dependent on ageing effects occurring by thermal treatments below T_g. These effects are studied using two complementary techniques: differential scanning calorimetry and dynamic mechanical spectroscopy at low frequencies ($1–10^{-4}$ Hz). Experimental results can be described through a physical model assuming diffusion and annihilation of 'quasi-point defects'. The distribution in the mobility of these defects is able to take into account all the phenomena observed after physical ageing, in particular the effects of low-temperature ageing. The ageing effects in the semicrystalline material cannot be deduced from those observed for the amorphous one by a single two-phase rule. Changes in the correlation factor of molecular movements and changes in the distribution of defects are necessary to describe all the observed effects, putting in evidence the role of the crystallites to reduce the segmental mobility.

(Keywords: poly(ethylene terephthalate); physical ageing; dynamic mechanical spectroscopy)

INTRODUCTION

Glassy polymers are known to have changes with time[1] in their physical and mechanical properties when annealed at temperatures close to, but below, their glass transition temperature T_g. The best-documented effects under these conditions are those involving primary thermodynamic properties such as specific volume or enthalpy, exhibiting both non-linear and thermal history effects[2–4]. However, many other properties of amorphous materials can be affected by physical ageing, in particular properties depending on molecular mobility. For example, dynamic mechanical properties are influenced by the isothermal approach to equilibrium in such a way that the loss tangent decreases and the storage modulus increases[5].

Semicrystalline materials also exhibit these so-called ageing effects, but it may be asked whether the glassy state of these materials undergoes the same ageing effects that would be found if isolated (i.e. as a purely glassy material). A recent review on this point has been developed by Struik[6] concerning the changes that occur in mechanical properties on ageing, and a model is proposed, assuming an extended glass transition zone in semicrystalline polymers.

Poly(ethylene terephthalate) (PET) is a well known polymer with important industrial applications, and it can be easily obtained either amorphous or semicrystalline in a wide range of crystallinity as a result of thermal treatments above the glass transition region. Physical ageing has been essentially studied in the amorphous state[7–13], showing no evidence of crystallization on ageing, and few results are available concerning the semicrystalline state[14].

The purpose of this paper is to study the kinetics of the return to equilibrium of the specific enthalpy and of the dynamic mechanical properties of amorphous and semicrystalline PET when isothermally annealed at temperatures below the glass transition temperature. Theoretical developments will be proposed in order to interpret the experimental data in a unique framework through a physical model assuming diffusion and annihilation of 'quasi-point defects'[4,15,16].

EXPERIMENTAL

Material

Amorphous films of PET (0.85 mm thick) were supplied by Rhone-Poulenc Films (molecular weight $M_n = 20\,000$). Density measurements, d.s.c. and X-ray diffraction analysis exhibit no measurable amount of crystallinity.

Semicrystalline specimens were obtained by isothermal crystallization of amorphous films of PET. The crystallization process was done at 393 K for 1 h. Crystallinity ratio was determined using a density gradient column containing an ethanol/carbon tetrachloride mixture[17] and assuming[18] the density of perfect crystalline PET to be 1.455 g cm^{-3} and that of amorphous material to be 1.355 g cm^{-3}. For this thermal treatment a crystallinity of 32% is obtained. SAXS experiments, according to Vonk's analysis[19], give access to the long period ($L_p = 8$ nm) and to the crystalline lamellae thickness ($L_c = 3.5$ nm). In PET, two different amorphous phases may coexist when crystallization occurs[20]. These two phases present different molecular mobility and can be distinguished as amorphous phase between spherulites and amorphous phase inside spherulites. In this study only fully crystallized PET will be investigated, i.e. material with amorphous phase principally located inside spherulites.

* To whom correspondence should be addressed

0032-3861/93/204257-10

Methods

Two characterization techniques were used to follow changes in the thermal and micromechanical properties of PET. Differential scanning calorimetry (d.s.c.) and dynamic mechanical spectroscopy (d.m.s.) experiments were performed as a function of sub-T_g annealing time and temperature.

A Mettler TA3000/DSC 30 instrument was used for d.s.c. study. D.s.c. scans were done at a 10 K min^{-1} heating rate between 293 and 373 K. Thermal treatments (annealing) were made directly in the sealed d.s.c. pan outside the d.s.c. apparatus.

Dynamic mechanical spectroscopy measurements were performed using an inverted torsional apparatus, working in the sub-resonant forced oscillations mode, developed in the laboratory[21]. It allows measurements of dynamic modulus ($G^* = G' + iG''$) and internal friction ($\tan \phi = G''/G'$) for frequencies between 1 and 10^{-4} Hz. The maximum amplitude of deformation is around 10^{-5} and *in situ* thermal treatments are possible.

The amorphous PET samples were heated to a temperature above T_g ($T = 368$ K) and annealed at that temperature for 15 min to erase any previous ageing. Density (density gradient column method) and X-ray diffraction measurements confirm that no crystallization has occurred as a result of this treatment. Thereafter specimens were quenched below T_g (at a rate of about 30 K min^{-1}), in a liquid nitrogen bath, then maintained at a sub-T_g annealing temperature for different ageing times (from 10^3 to 10^6 s). The ageing temperatures were 303, 318 and 333 K.

For the semicrystalline materials, specimens were directly quenched after crystallization to the ageing temperature where they were maintained for different ageing times (from 10^3 to 10^6 s). The ageing temperatures were the same as for the amorphous material.

EXPERIMENTAL RESULTS

D.s.c. thermograms for amorphous PET are shown in *Figure 1* for different ageing temperatures T_a and ageing times t_a. The curve corresponding to non-aged specimen is obtained after cooling from 368 K at 0.5 K s^{-1} for the amorphous specimens and from 393 K at the same cooling rate for semicrystalline specimens. These curves will be taken as reference curves to calculate the residual enthalpy.

For low-temperature annealing ($T_a = 303$ K), the ageing effect is only visible for an ageing time over 10^5 s and the endothermic enthalpy recovery peak appears well below T_g. As the ageing temperature increases, this peak developed sooner, first shifted towards low temperatures for short ageing time (10^3 s). When ageing times increase, the endothermic peak moves towards high temperatures, increasing its amplitude.

The variation of the endothermic peak temperature depends on the ageing conditions; in particular, low-temperature ageing is known to give a peak located at temperatures below the classical T_g. Phenomenological relations proposed by different authors[22–24] are able to describe the variation in temperature of the endothermic peak and a sub-T_g endothermic peak can be explained using a distribution of relaxation times[22].

From these thermograms, residual enthalpy H_r can be determined by taking the difference between the curve corresponding to the non-aged state and the curves

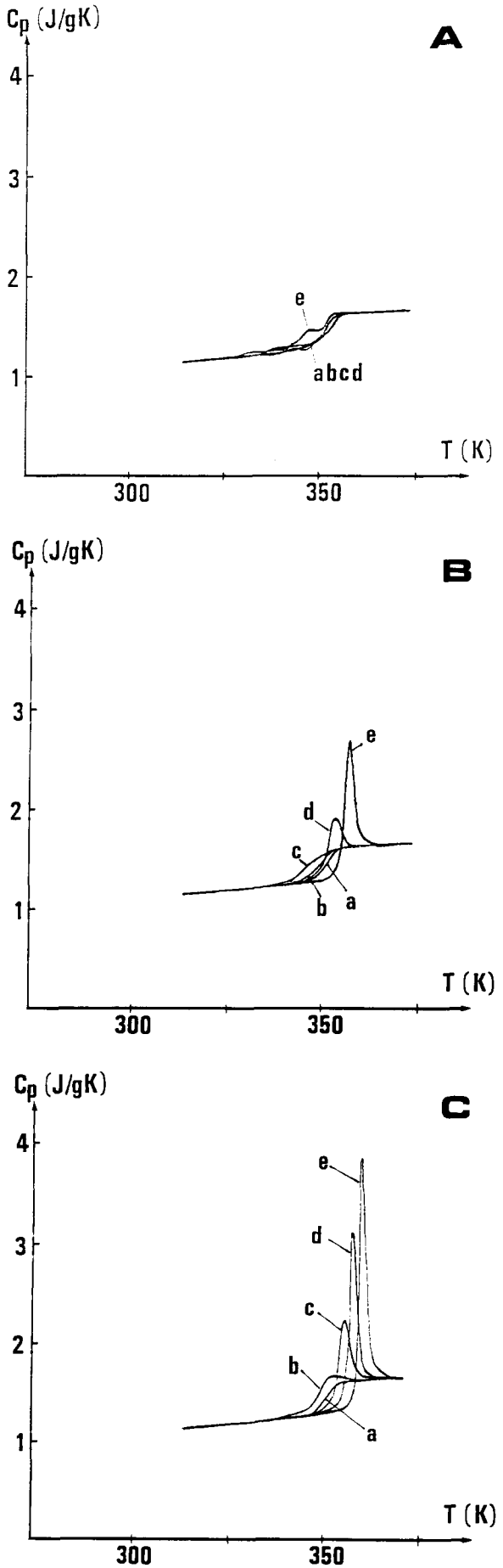

Figure 1 D.s.c. thermograms ($dT/dt = 10$ K min^{-1}) of amorphous PET. The three parts are for different ageing temperatures: (A) $T_a = 303$ K, (B) $T_a = 318$ K, (C) $T_a = 333$ K. The various curves show ageing times: (a) without ageing, (b) 10^3 s, (c) 10^4 s, (d) 10^5 s, (e) 10^6 s

corresponding to different aged states. As an example, *Figure 2* presents the evolution of H_r as a function of time for an ageing temperature of 333 K. The evolution is nearly complete at 10^6 s for this temperature.

In the case of semicrystalline PET (*Figure 3*), ageing effects are not so easy to see. At 303 K, no ageing effect can be distinctly observed and within the experimental dispersion no changes can be seen compared to the reference curve until the ageing time is 10^6 s. For annealing at $T_a = 318$ K, a sub-T_g endothermic peak becomes visible after 10^5 s and we can observe the classical shift towards high temperature as ageing time increases.

When ageing at high temperature ($T_a = 333$ K), the ageing effects appear as soon as $t_a = 10^3$ s. Even when ageing time increases (up to 10^6 s), the temperature of the endothermic peak remains below T_g obtained with the non-aged specimen. As in the case of amorphous PET (see *Figure 1* for comparison), the peak is shifted towards high temperature and its amplitude grows when the ageing time increases.

It is also noticeable that the temperatures corresponding to the end of glass transition (i.e. when metastable equilibrium is reached) are higher than in the case of the amorphous material. This shift is about 15 K whereas the temperature of the beginning of the glass transition (onset point) does not differ very much from those of wholly amorphous material. So, in the case of semicrystalline material the glass transition phenomenon is spread on a larger domain of temperature and the behaviour near T_g cannot be deduced directly from those of amorphous material, using a simple proportional two-phase rule. Only the ΔC_p value above T_g is proportional to the amorphous phase ratio in the material.

Dynamic mechanical spectroscopy measurements are presented in *Figure 4* for the amorphous material. The dependence of tan ϕ on temperature is shown for different frequencies between 100 and 375 K. As previously observed by different authors[25,26], two mechanical relaxations can be observed:

(i) at high temperature (385 K/1 Hz), the main or α relaxation associated with the glass transition, whose apparent activation energy in this domain of frequencies is equal to 640 kJ mol^{-1}; and

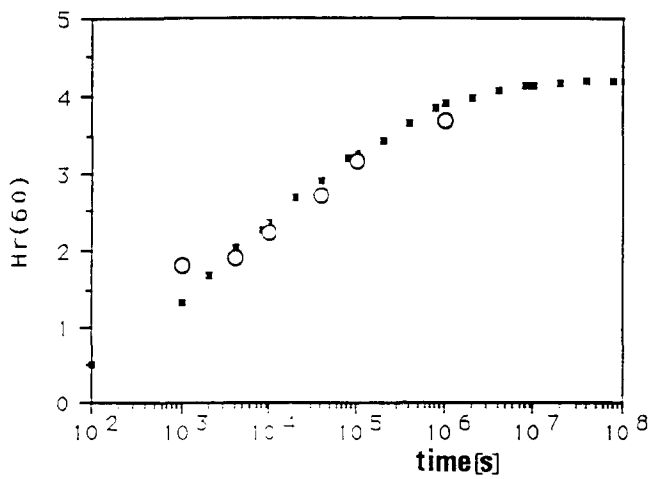

Figure 2 Evolution of the residual enthalpy H_r as a function of ageing time at $T_a = 333$ K for amorphous PET: (○) experimental data, (■) theoretical results

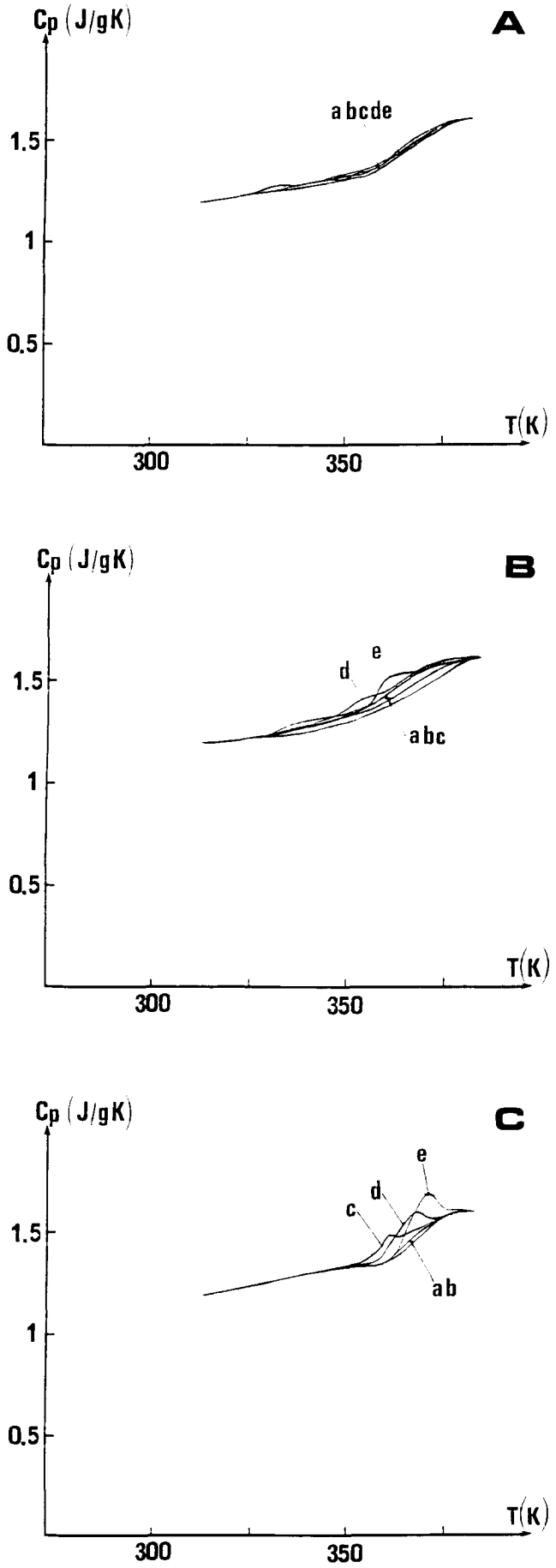

Figure 3 D.s.c. thermograms ($dT/dt = 10$ K min^{-1}) of semicrystalline PET ($X_c = 32\%$). Ageing temperatures: (A) $T_a = 303$ K, (B) $T_a = 318$ K, (C) $T_a = 333$ K. Ageing times: (a) without ageing, (b) 10^3 s, (c) 10^4 s, (d) 10^5 s, (e) 10^6 s

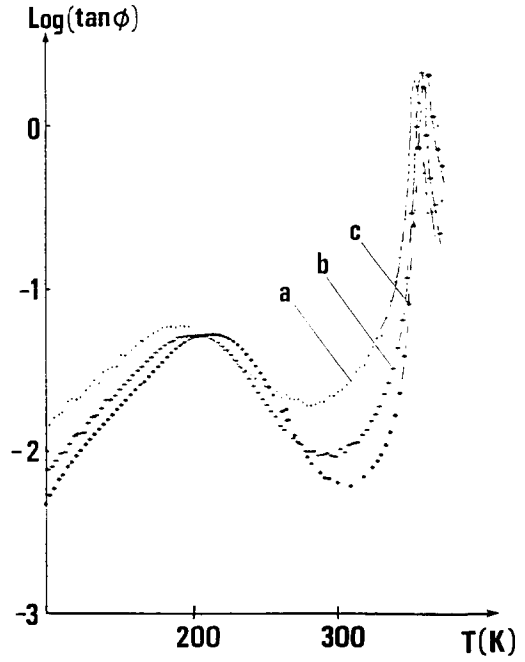

Figure 4 Internal friction (tan ϕ) vs. temperature for amorphous PET: (a) 0.01 Hz, (b) 0.1 Hz, (c) 1 Hz

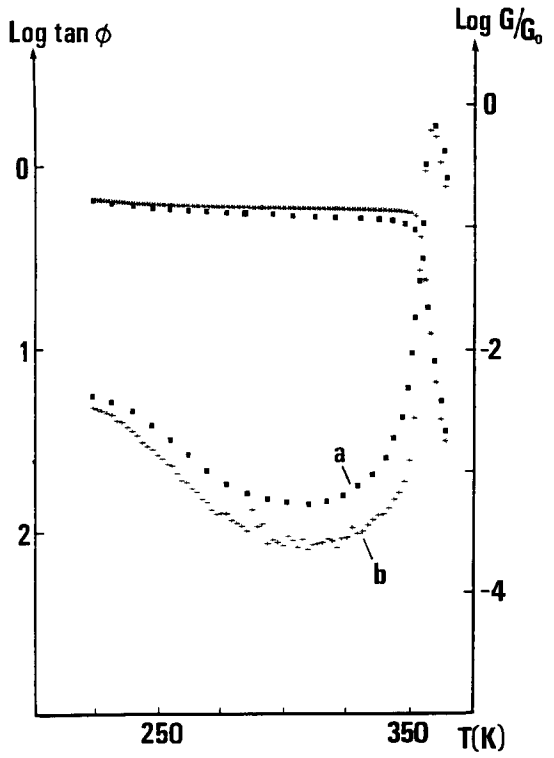

Figure 5 Effect of ageing on tan ϕ for amorphous PET: (a) non-aged; (b) effect of ageing (aged 60 h at 333 K)

(ii) at low temperature (200 K/1 Hz), the secondary or β relaxation, which was attributed[15] to complex relaxations of different groups in the polymer chain, and whose apparent activation energy was found to be equal to 63 kJ mol^{-1}.

The effects of sub-T_g annealing are shown on *Figure 5* for ageing treatments at $T_a = 333$ K for 60 h. The only part of the spectra affected by ageing is that located between the β and α relaxations, where a decrease of tan ϕ is observed after ageing. The low-temperature part of the secondary relaxation peak is unaffected by thermal treatments below T_g, which confirms previous results[27].

When internal friction is recorded in isothermal conditions ($T = T_a$) as a function of ageing time, kinetic curves are obtained as shown on *Figure 6*. The structural relaxation rate is considerably slowed when ageing time reaches 10^5 s.

Dynamic mechanical spectroscopy measurements are presented in *Figure 7* for the semicrystalline material without ageing. The temperature and the width of the β relaxation are not affected by the crystalline phase. The apparent activation energy remains constant. The β relaxation intensity (β peak area) decreases but not proportionally to the amorphous phase ratio. On the contrary, the α relaxation is shifted towards higher temperature (about 10°C) and the α peak

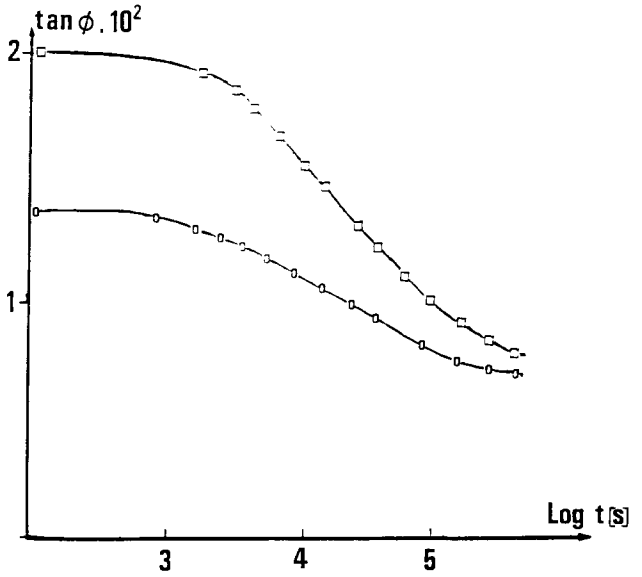

Figure 6 Evolution of tan ϕ with ageing time ($T_a = 333$ K): (□) 1 Hz, (○) 0.1 Hz

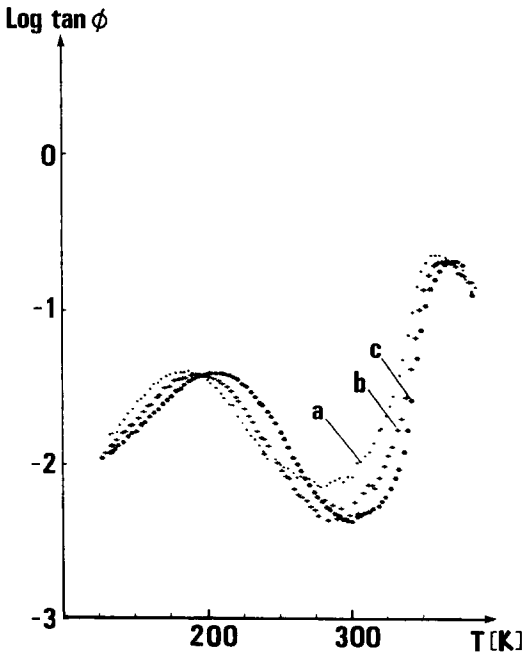

Figure 7 Internal friction (tan ϕ) vs. temperature for semicrystalline PET: (a) 0.01 Hz, (b) 0.1 Hz, (c) 1 Hz

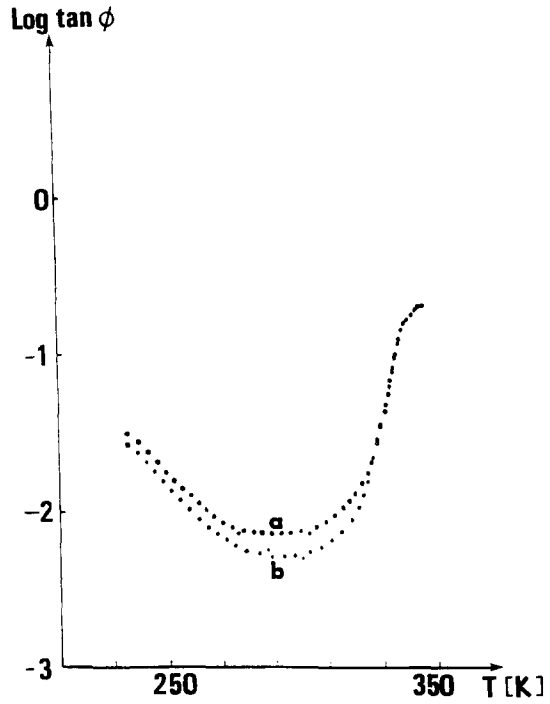

Figure 8 Effect of ageing on tan ϕ for semicrystalline PET: (a) non-aged; (b) effect of ageing (aged 60 h at 333 K)

broadens. The α intensity relaxation is nearly proportional to the amorphous phase ratio. The internal friction between α and β peak relaxations decreases strongly (2×10^{-2} in the amorphous state against 8×10^{-3} in the semicrystalline state).

The effect of sub-T_g annealing is shown in *Figure 8* for ageing treatment at $T_a = 333$ K for 60 h. As in the amorphous state, the only part affected by ageing is located between the β and α relaxations, but the decrease of tan ϕ is much smaller.

DISCUSSION

In previous works[4,16] a physical interpretation of the structural relaxation observed near to, but below, T_g was proposed. The model is based on the principal assumption that density fluctuations in a glassy polymer can be considered as 'quasi-point defects'. These defects, when ageing does not occur, are frozen for $T < T_g$ and by the usual arguments of statistical thermodynamics their concentration in metastable conditions is given by:

$$C_d = \frac{1}{1 + \exp(-S_F/k)\exp(H_F/kT)} \quad (1)$$

where S_F and H_F are respectively the entropy and the enthalpy of formation of these defects.

The structural relaxation at $T_a < T_g$ could be interpreted in terms of diffusion-aided annihilation of defects until a new thermodynamic (metastable) equilibrium is reached at this temperature. This diffusion involves hierarchically correlated movements[28,29] and the relaxation time τ_i of each type of defect movement can be expressed by[29]:

$$\tau_i = (\tau_\beta / t_0^{b_i - 1})^{1/b_i} \quad (2)$$

where τ_β is the relaxation time of an elementary process, and will be taken as the relaxation time of the β relaxation, and b_i is a correlation factor, which characterizes the degree of correlation of each type of defect movement. In other words, the mobility of each type of defect will depend on its environment via the correlation factor b_i. Then the structural relaxation can be described by a set of differential equations related to the evolution of each type of defect population:

$$dC_{d_i} = \frac{C_{d_i}(t) - C_{d_i}(eq)}{\tau_i} dt \quad (3)$$

According to the model[16], a relation exists between b, the mean value of the correlation factor, and C_d, the global concentration of quasi-point defects:

$$b = \frac{1}{1 + b_0 \exp(-A^* C_d)} \quad (4)$$

where b_0 and A are parameters depending on the nature and morphology of the material.

For simplification in the numerical calculations, the distribution over the mobility of the defects (i.e. distribution of $1/b_i$) is taken as Gaussian and can be written as:

$$g_i = \frac{1}{B_g \pi^{1/2}} \exp\left[-\left(\frac{1}{b_i} - \frac{1}{b}\right)^2 \Big/ B_g \right] \quad (5)$$

where $C_d = \sum_{g_i} C_{d_i}$.

Let us remark that the distribution of $1/b_i$ corresponds to a Gaussian distribution of the relaxation times τ_i.

So, numerical calculations of equations (2) will allow one, through (5), (3) and (1), to obtain the concentration of each kind of defect during the process. As:

$$C_p = H_F (dC_d/dT) N_A \quad (6)$$

N_a = Avogadro's number, it will be possible to simulate d.s.c. experiments.

The different parameters are determined from either d.s.c. or dynamic mechanical spectroscopy experiments and determinations are detailed in previous papers[4,29]. Values for H_F and S_F are obtained from[4] $\Delta C_p = C_p(\text{liq}) - C_p(\text{glass})$ at $T = T_g$. An experimental value of $\Delta C_p = 0.4$ J g^{-1} K^{-1} leads to $H_F = 13.4$ kJ mol^{-1} and $S_F = 2.15k$.

Dynamic mechanical spectroscopy measurements on amorphous PET give access to τ_β, as $\tau_\beta = t_1 \exp(U_\beta/kT)$ from the β relaxation process ($t_1 = 10^{-15}$ s, $U_\beta = 63$ kJ mol^{-1}). From a Cole–Cole diagram (G'' vs. G'), a value of b is obtained[29] ($b = 0.34$ at $T = 348$ K). Through relation (1) a value of C_d at this temperature can be deduced, giving access to pairs of values (b_0, A). Comparisons between experimental and d.s.c. curves for different ageing times and temperatures allow the adjustment of these curves for a unique value of B_g and a particular pair A, b_0. The characteristic time t_0 acts as a scaling factor and will be taken equal to 7×10^{-10} s. Numerical simulations have been done using 21 types of defect environments in the distribution, corresponding to a calculation step $\Delta(1/b_i) = 0.15$.

For the amorphous material, the distribution factor B_g is equal to 0.31 with $A = 15$ and $b_0 = 8.6$, and the simulated d.s.c. thermograms are shown in *Figure 9* with ageing treatments corresponding to those carried out experimentally. A very good agreement is found for high-temperature ageing treatments, i.e. 333 K; in particular the location of the maximum of the endothermic peak and its shifts with ageing times are well found. The agreement is not so good for ageing at low temperatures, but the simulated curves exhibit a sub-T_g peak close to the experiments. From considerations about the differential equations (3)

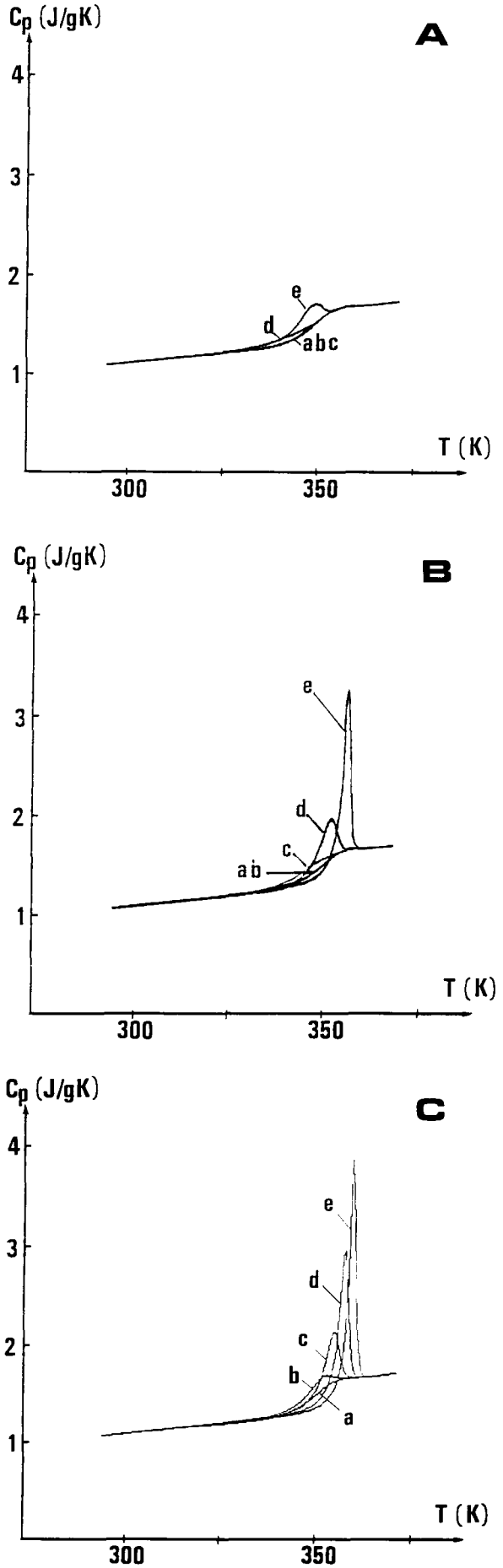

Figure 9 Calculated d.s.c. thermograms for amorphous PET: (A) $T_a = 303$ K, (B) $T_a = 318$ K, (C) $T_a = 333$ K; (a) without ageing, (b) 10^3 s, (c) 10^4 s, (d) 10^5 s, (e) 10^6 s

describing the structural relaxation through the defect concentrations, it is possible to explain the displacement of the endothermic peak when ageing time increases. In effect, for an ageing temperature T_a close to T_g, ageing treatment produces two dual effects:

(i) an increase of the difference $(C_{d_i}(\text{eq}) - C_{d_i}(t))$ at the temperatures where the endothermic peak can occur; and

(ii) a decrease of the correlation factor b_i (movement becomes more difficult as defects are annihilated). This last effect corresponds to an increase of τ_i.

These two effects are opposed, so we can understand the displacement towards low temperatures for short ageing times (first effect is preponderant) but when ageing times become longer the maximum of C_p is observed at higher temperature as the effect on mobility then becomes preponderant.

With the above parameters fixed, it is possible also to obtain the histograms of the defect distributions all along the thermal treatments (quenching from above T_g, ageing treatments, heating at the same rate as in d.s.c. experiments). An example of such calculations is given in *Figure 10* when quenching from 368 K to ageing temperature of 333 K at a rate of 0.5 K s^{-1} is simulated. From the initial state where defects have a Gaussian distribution of their mobility, it appears that quenching leads to a non-symmetrical distribution where less-mobile defects are far from the equilibrium concentration at this temperature. During ageing at 333 K, an evolution towards equilibrium occurs, and the higher the defect mobility, the shorter is the time to reach this equilibrium. As shown in *Figure 11* after 10^6 s the metastable equilibrium is nearly obtained.

Calculations of the residual enthalpy are also possible according to the model, and in *Figure 2*, H_r was plotted *versus* ageing time for $T_a = 333$ K and compared to experimental results.

When ageing occurs at low temperature, for example at 303 K, the dissymmetry becomes more important than at 333 K; especially the less-mobile defects are far from their equilibrium even for long ageing time (*Figure 12*).

For a qualitative explanation concerning the occurrence of a sub-T_g endothermic peak when ageing treatment is carried out at low temperature (i.e. 303 K), we have plotted in *Figure 13* the evolution, after the same time (10^6 s) and on heating (d.s.c. experiment rate = 10 K min^{-1}), of the concentration of defects with different mobilities. The population no.10 is representative of the average of the initial distribution, whereas nos. 7 and 9 and nos. 11 and 13 are respectively representative of more- and less-mobile defects. When ageing is performed at 333 K, the figure indicates clearly that the enthalpy that gives the endothermic peak in C_p (proportional to dC_d/dt) is released very quickly in an interval of temperature of 2 K for all the defects, whatever their mobility. At a temperature just before the endothermic peak, all the defect concentrations are lower than their equilibrium concentration; but as the temperature increases, the defect mobility increases also; then the defects tend to reach their equilibrium concentration, and therefore their number increases; and this phenomenon also increases the mobility, and so on: an 'avalanche' phenomenon occurs, which explains the existence of the very sharp endothermic peak. On the contrary, when ageing is done at 303 K the enthalpy has a fast evolution only for defects whose mobility is high and at temperatures below T_g. (The arrows refer to sub-T_g

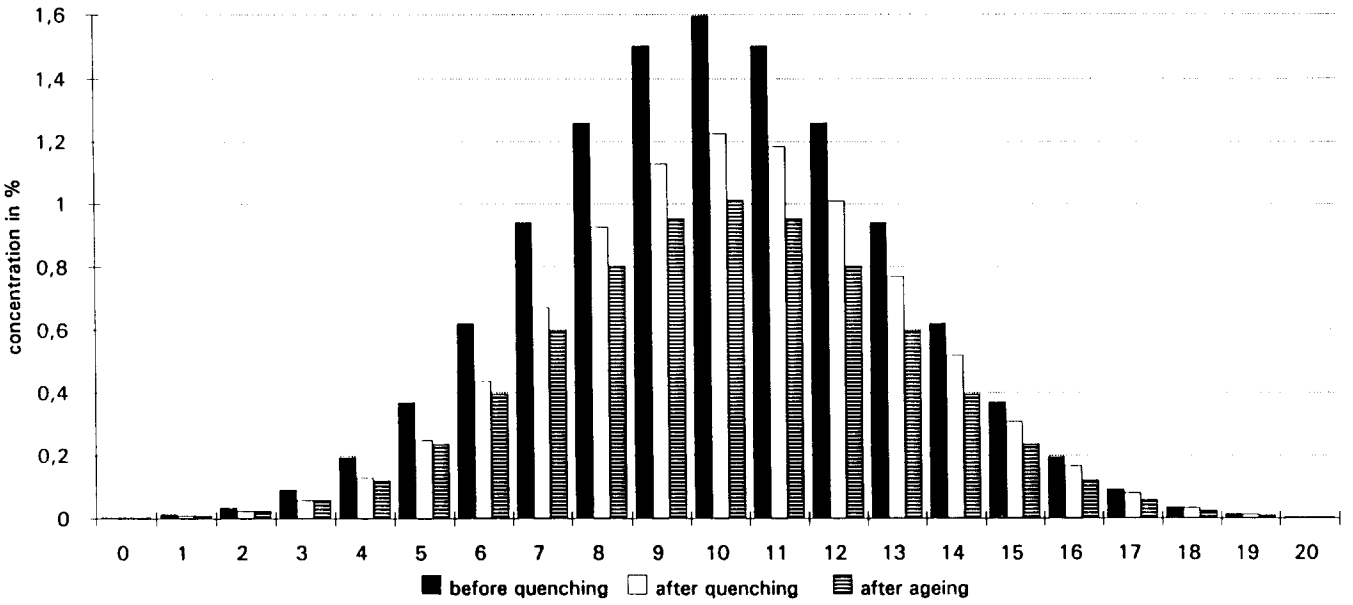

Figure 10 Distribution of defect concentrations (mobility decreases from class 0 to 20): before quenching ($T = 368$ K), after quenching at 333 K, and after ageing (10^6 s at 333 K)

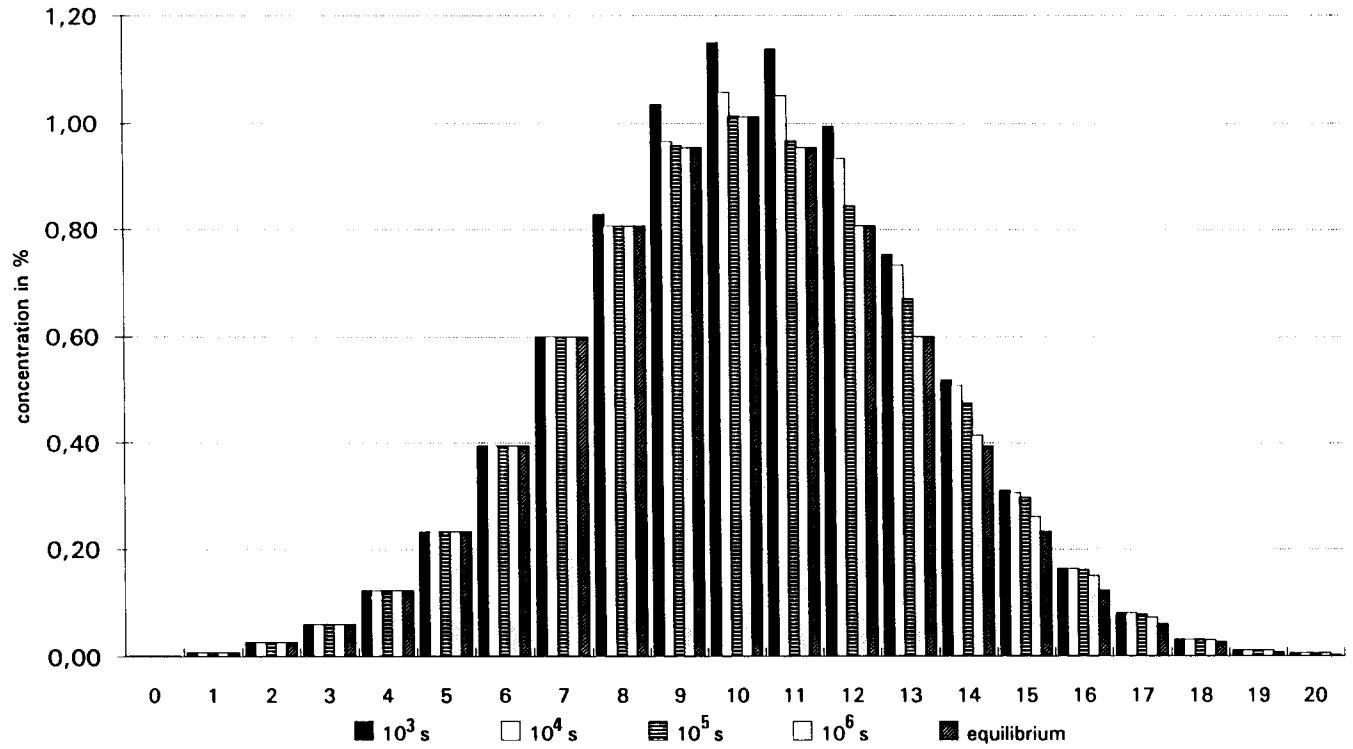

Figure 11 Evolution of defect populations when ageing at 333 K for various times

peak and to peak temperatures.) At a temperature just before the sub-T_g peak (348 K), the more-mobile defect concentrations are lower than their equilibrium, whereas, on the contrary, the less-mobile defect concentrations are higher than their equilibrium concentration (see *Figure 12*). Therefore, as the temperature increases, only the more-mobile defect concentrations increase, leading to the sub-T_g peak.

To develop simulations in the case of semicrystalline PET, we let the parameters related to intrinsic properties of defects (S_F, H_F, τ_β, t_0) be the same as for amorphous PET. There are no physical reasons to think that these parameters are influenced by the occurrence of a crystalline phase. In particular, the mechanical β relaxation has the same physical characteristics (τ_β) when the material becomes semicrystalline[30].

To obtain a correct simulation of d.s.c. thermograms in semicrystalline PET, only two types of parameters have been modified:

(i) The parameters in the relation giving b from C_d. For the same defect concentrations, the molecular mobility will be different in semicrystalline PET. In effect, owing to the small thickness of amorphous zone between

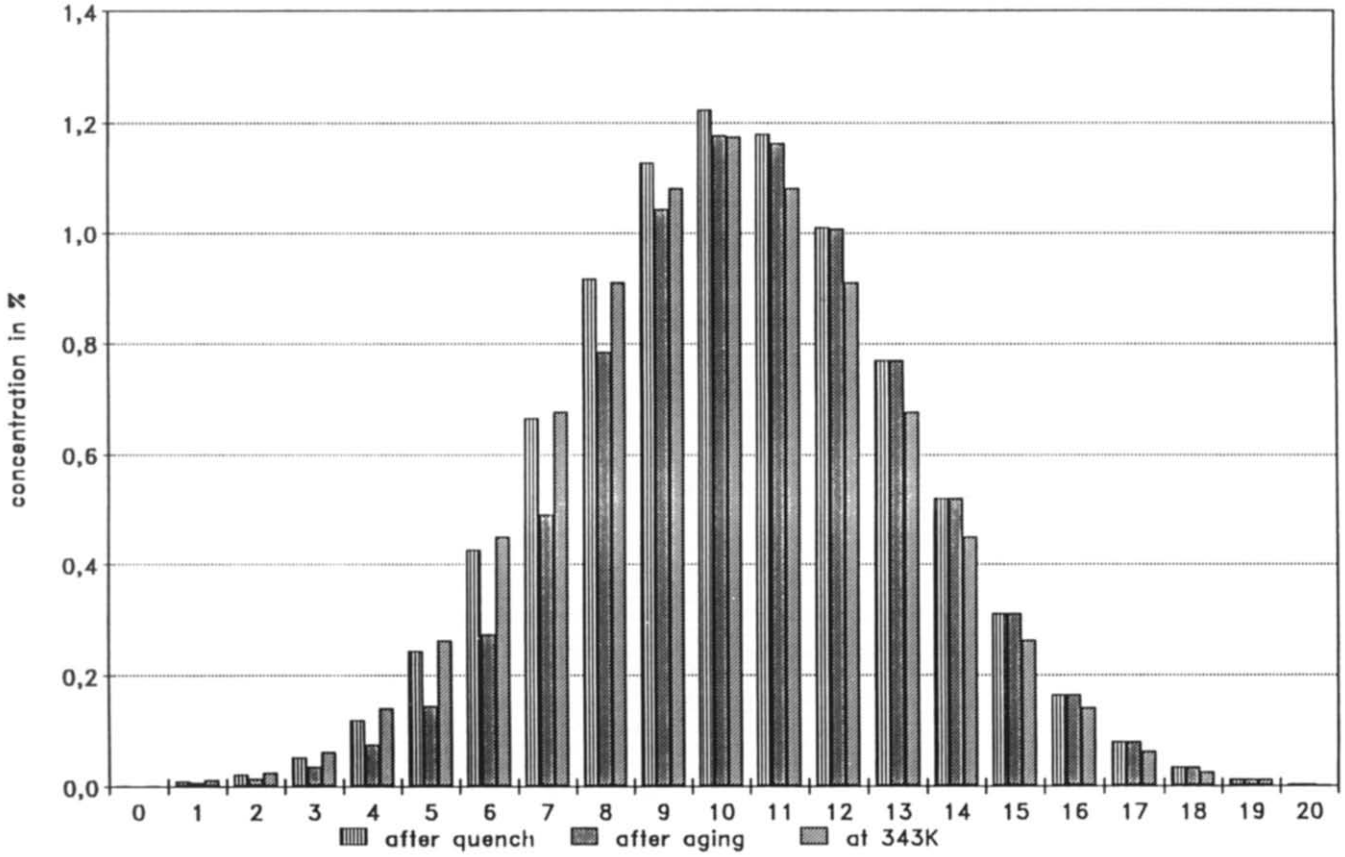

Figure 12 Distribution of defect concentrations after ageing at low temperature: after quenching (T= 303 K), after ageing (10^6 s at 303 K), and at metastable equilibrium at 343 K

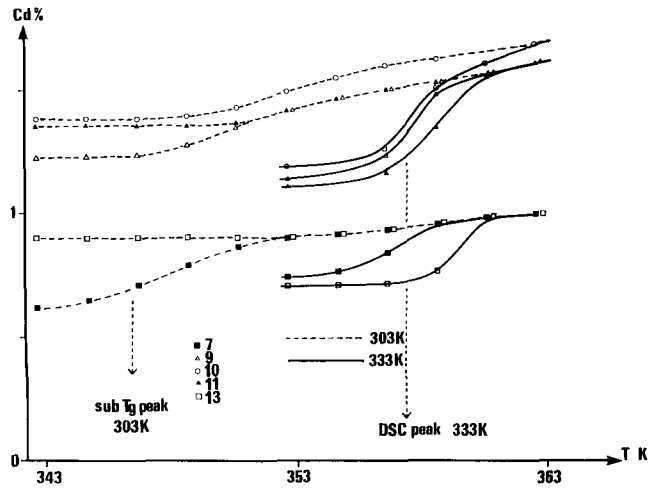

Figure 13 Evolution of different defect populations after ageing at 333 K and 303 K when heating at 10 K min^{-1}: (7) and (9) more-mobile defects; (10) averagely mobile defects; (11) and (13) less-mobile defects

crystalline lamellae (3.5 nm), there is a great probability that the majority of chains involved in the amorphous phase belong also to adjacent crystalline lamellae and are 'anchored' to the crystalline phase. Their mobility is reduced, which is confirmed by the evolution of the parameters:

amorphous	semicrystalline
$A=15$	$A=7$
$B_0=8.6$	$B_0=6$

For the same value of C_d (taken as 0.1) the corresponding values of b are respectively 0.34 for the amorphous PET and 0.25 for the semicrystalline PET. The decrease of b with crystallinity indicates a stronger correlation, that is to say that segmental mobility is reduced.

(ii) The parameter that characterizes the distribution of defect mobility (B_g). In order to have the best adjustment we have to choose a higher value for B_g ($B_g=0.60$) compared to a value of 0.31 when the material is fully amorphous. Such a value means that the mobility of defects is less regularly distributed than in the case of amorphous PET. One can think that, inside the amorphous phase between the crystalline lamellae, the defects are principally located near the centre of this zone, and that the vicinity of crystalline lamellae has to be considered as a defect-depleted zone with respect to molecular chains participating in both phases.

With such modifications in the parameters of the model, simulations of d.s.c. thermograms are possible, and *Figure 14* shows simulated curves for corresponding ageing temperatures. If the calculated curves are difficult to compare to experimental results for $T_a=303$ and 318 K, as the ageing effects are small, when $T_a=333$ K a rather good agreement is obtained, despite the amplitude of the sub-T_g endothermic peak obtained for 10^6 s. Nevertheless, temperatures of peaks are in good coincidence with experiments.

A model for the description of dynamic mechanical properties is only proposed for the amorphous material; in effect the existence of crystallites makes the problem more complex; a work concerning d.m.s. properties of semicrystalline PET will be presented later.

According to a previous description of the complex

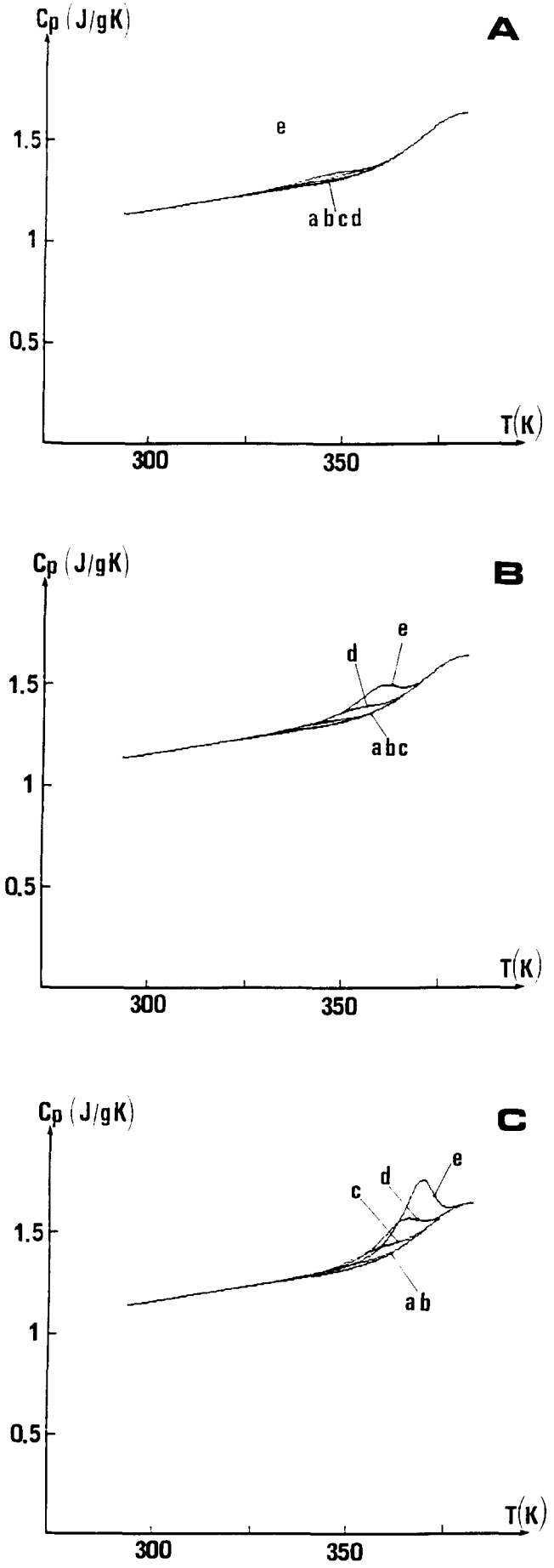

Figure 14 Calculated d.s.c. thermograms for semicrystalline PET: (A) $T_a = 303$ K, (B) $T_a = 318$ K, (C) $T_a = 333$ K; (a) without ageing, (b) 10^3 s, (c) 10^4 s, (d) 10^5 s, (e) 10^6 s

modulus[29], we can write:

$$G^*(i\omega) = G'(\omega) + iG''(\omega)$$

$$G^*(i\omega) = G_r + \frac{G_u - G_r}{1 + (i\omega\tau_r)^{-b} + c(i\omega\tau_r)^{-h}}$$

and it has been shown that:

$$\tau_r = (\tau_\beta / t_0^{b-1})^{1/b} (AG_u/b)^{-1/b}$$

$$c = (b^{h/b}/h)(AG_u)^{-(h/b-1)}$$

where G_u and G_r are respectively the unrelaxed and relaxed modulus, b the mean correlation factor previously described, h a constant obtained from the slope at zero frequency of the Cole–Cole plot and A an adjustable parameter.

So it is possible to simulate the dynamic mechanical spectroscopy experiments, especially for the α relaxation zone with the assumption that the β relaxation process is independent of the α relaxation. With the same set of parameters used in our d.s.c. simulations and with a value $h = 0.8$, G_u and G_r taken respectively equal to 7×10^8 Pa and 4×10^6 Pa, it is possible to calculate G', G'' and tan ϕ. *Figure 15* shows a comparison between the isothermal master curve of tan ϕ measured at 348 K and the theoretical curve. The fit is reasonably good around the peak value but becomes less satisfactory towards higher frequencies. This may be attributed to the fact that the weak contribution from the β relaxation is not taken into account in our calculations and/or the assumption of an average value for β in the use of $G'(\omega)$ and $G''(\omega)$.

For a given frequency (1 Hz) it is also possible to obtain isochronal curves of tan ϕ for the contribution of the α relaxation, and *Figure 16* shows the effect of ageing treatment (10^6 s at 333 K) on this spectrum. As in our experiments, ageing affects only the low-temperature range of the α relaxation, the two curves merging at a temperature ($T = 352$ K) where metastable equilibrium is reached.

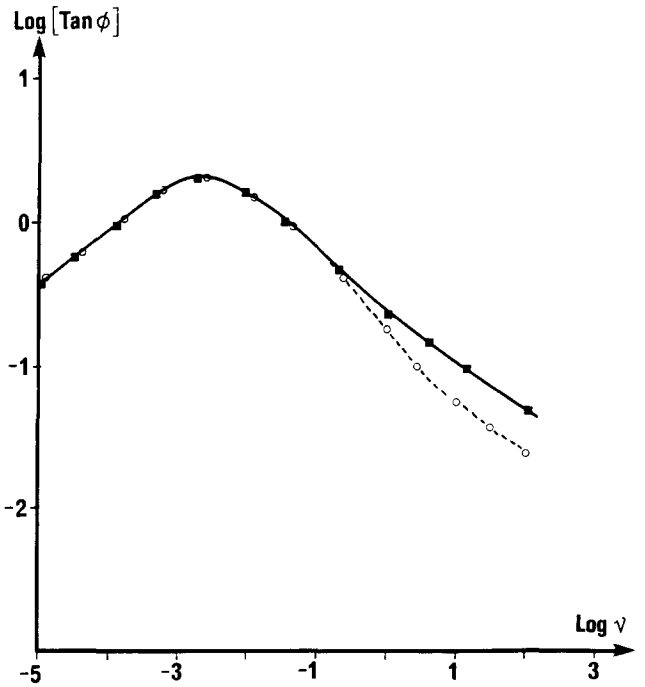

Figure 15 Plot of tan $\phi = G''/G'$ vs. frequency at $T = 348$ K (non-aged specimen): (○) calculated, (■) experiments

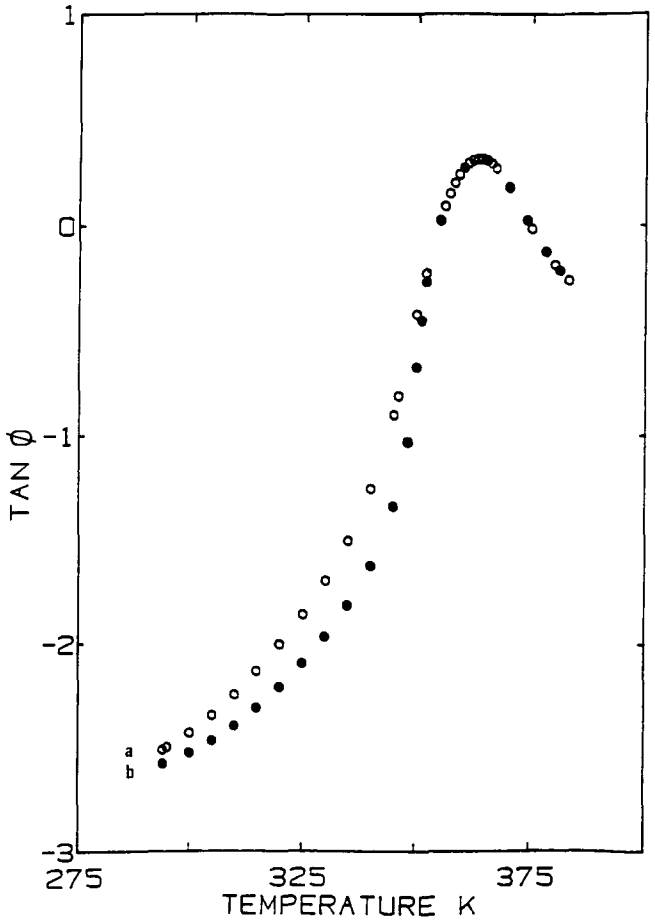

Figure 16 Plot of tan ϕ vs. temperature, calculated curves (1 Hz): (○) non-aged, (●) aged 60 h at $T = 333$ K

CONCLUSION

Physical ageing in amorphous and semicrystalline poly(ethylene terephthalate) has been studied experimentally by two complementary techniques, d.s.c. and d.m.s.

The 'quasi-point defects' model, improved by a distribution of the mobility of the defects, is able to describe the structural relaxation of the amorphous material and with the same set of parameters to simulate both d.s.c. and d.m.s. experiments. Considerations on the histograms of defect populations give qualitative explanations of the different aspects of the phenomenon (displacement of the endothermic peak, sub-T_g peak, ...).

The same model can explain the results obtained for the semicrystalline material. By keeping intrinsic parameters of defects (S_F, H_F, τ_β, t_0) the same as in the case of the fully amorphous material and by changing only parameters related to correlated motion of defects (b) and to distribution of defect mobility (B_g), a rather good agreement is found with experiments.

Variations of these parameters appear to have a physical meaning and show that the segmental mobility in the amorphous phase located between crystalline lamellae is quite different from that in the bulk amorphous phase.

REFERENCES

1 Struik, L. C. E. 'Physical Aging in Amorphous Polymers and Other Materials', Elsevier, Amsterdam, 1978
2 Kovacs, A. J. *Adv. Polym. Sci.* 1963, **3**, 374
3 Kovacs, A. J. *J. Polym. Sci.* 1958, **30**, 131
4 Perez, J. *Polymer* 1988, **29**, 483
5 Perez, J., Cavaille, J. Y., Diaz-Calleja, R., Ribelles, J. L., Pradas, M. M. and Ribes Greus, A. *Makromol. Chem.* 1991, **192**, 2141
6 Struik, L. C. E. *Polymer* 1987, **28**, 1521, 1534; *Polymer* 1989, **30**, 799, 815
7 Siegman, A. and Turie, E. *J. Macromol. Sci.–Phys.* (*B*) 1974, **10** (4), 689
8 Aref-Azar, A. and Hay, J. N. *Polymer* 1982, **23**, 1129
9 Aref-Azar, A., Biddlestone, F., Hay, J. N. and Haward, R. N. *Polymer* 1983, **24**, 1245
10 Ito, E., Tajima, K. and Kobayashi, Y. *Polymer* 1983, **24**, 877
11 Montserrat, S. and Cortes, P. *Anal. Quim.* 1986, **82**, 499
12 Cortes, P. and Montserrat, S. *Makromol. Chem., Makromol. Symp.* 1989, **27**, 279
13 Petrie, S. E. B. *J. Macromol. Sci.-Phys.* (*B*) 1976, **12**, 225
14 Tant, M. R. and Wilkes, G. L. *J. Appl. Polym. Sci.* 1981, **26**, 2813
15 Perez, J. *Solid State Ionics* 1990, **39**, 69
16 Perez, J., Cavaille, J.-Y. and Tatibouet, J. *J. Chim. Phys.* 1990, **87**, 1923
17 Wunderlich, B. 'Macromolecular Physics', Academic Press, New York, 1973, Vol. 1, p. 382
18 Daubeny, R. De P., Bunn, C. W. and Brown, J. C. *Proc. R. Soc.* (*A*) 1954, **226**, 531
19 Vonk, C. G. and Kortleve, G. *Kolloid Z. Z. Polym.* 1967, **220**, 19
20 Vigier, G., Tatibouet, J., Benatmane, A. and Vassoille, R. *Colloid Polym. Sci.* 1992, **270**, 1182
21 Etienne, S., Cavaille, J.-Y., Perez, J., Point, R. and Salvia, M. *Rev. Sci. Instrum.* 1982, **53**, 1251
22 Ramos, A. R., Hutchinson, J. M. and Kovacs, A. J. *J. Polym. Sci., Polym. Phys. Edn* 1984, **22**, 1655
23 Kovacs, A. J. and Hutchinson, J. M. *J. Polym. Sci., Polym. Phys. Edn.* 1979, **17**, 2031
24 Moynihan, C. T. *Ann. NY Acad. Sci.* 1976, 279
25 Illers, K. M. and Breuer, H. *J. Colloid Sci.* 1968, 18
26 Elsayed, S. and De Batist, R. *J. Physique* 1987, **48**, C8, 501
27 Struik, L. C. E. *Polymer* 1987, **28**, 57
28 Palmer, R. G., Stein, D. L., Abrahams, E. and Anderson, P. W. *Phys. Rev. Lett.* 1984, **53**, 958
29 Cavaille, J.-Y., Perez, J. and Johari, G. P. *Phys. Rev.* (*B*) 1989, **39**, 2411
30 Vigier, G., Muzeau, E., Mangion, M. B. M., Tatibouet, J., Vassoille, R. and Perez, J. Proc. ICIFUAS6, 1991, Cracow, Poland